EBioMedicine 44 (2019) 112–125

Contents lists available at ScienceDirect

EBioMedicine

journal homepage: www.ebiomedicine.com

EBioMedicine
Published by THE LANCET

Research paper

High-frequency irreversible electroporation is an effective tumor ablation strategy that induces immunologic cell death and promotes systemic anti-tumor immunity

Veronica M. Ringel-Scaia [a,b], Natalie Beitel-White [c,d], Melvin F. Lorenzo [c,e], Rebecca M. Brock [a,b], Kathleen E. Huie [b], Sheryl Coutermarsh-Ott [b], Kristin Eden [b,f], Dylan K. McDaniel [b], Scott S. Verbridge [e,h], John H. Rossmeisl Jr [h,i], Kenneth J. Oestreich [a,b,g,h,j], Rafael V. Davalos [a,c,e,f,h], Irving C. Allen [a,b,f,h,*]

[a] Graduate Program in Translational Biology, Medicine, and Health, Virginia Tech, Blacksburg, VA, USA
[b] Department of Biomedical Sciences and Pathobiology, Virginia Tech, Virginia-Maryland College of Veterinary Medicine, Blacksburg, VA, USA
[c] Bioelectromechanical Systems Laboratory, Department of Biomedical Engineering and Mechanics, Virginia Polytechnic Institute and State University, Blacksburg, VA, USA
[d] Department of Electrical and Computer Engineering, Virginia Tech, Blacksburg, VA, USA
[e] Virginia Tech - Wake Forest University, Virginia Tech, School of Biomedical Engineering & Sciences, Blacksburg, VA, USA
[f] Department of Basic Science Education, Virginia Tech Carilion School of Medicine, Roanoke, VA, USA
[g] Department of Internal Medicine, Virginia Tech Carilion School of Medicine, Roanoke, VA, USA
[h] Center for Engineered Health, Virginia Tech, Institute for Critical Technology and Applied Science, Blacksburg, VA, USA
[i] Department of Small Animal Clinical Sciences, Virginia-Maryland College of Veterinary Medicine, Blacksburg, VA, USA
[j] Virginia Tech, Fralin Biomedical Research Institute at Virginia Tech Carilion, Roanoke, VA, USA

ARTICLE INFO

Article history:
Received 5 March 2019
Received in revised form 14 May 2019
Accepted 14 May 2019
Available online 23 May 2019

Keywords:
IRE
Breast cancer
Metastasis
Tumor microenvironment
Pyroptosis

ABSTRACT

Background: Despite promising treatments for breast cancer, mortality rates remain high and treatments for metastatic disease are limited. High-frequency irreversible electroporation (H-FIRE) is a novel tumor ablation technique that utilizes high-frequency bipolar electric pulses to destabilize cancer cell membranes and induce cell death. However, there is currently a paucity of data pertaining to immune system activation following H-FIRE and other electroporation based tumor ablation techniques.
Methods: Here, we utilized the mouse 4T1 mammary tumor model to evaluate H-FIRE treatment parameters on cancer progression and immune system activation *in vitro* and *in vivo*.
Findings: H-FIRE effectively ablates the primary tumor and induces a pro-inflammatory shift in the tumor microenvironment. We further show that local treatment with H-FIRE significantly reduces 4T1 metastases. H-FIRE kills 4T1 cells through non-thermal mechanisms associated with necrosis and pyroptosis resulting in damage associated molecular pattern signaling *in vitro* and *in vivo*. Our data indicate that the level of tumor ablation correlates with increased activation of cellular immunity. Likewise, we show that the decrease in metastatic lesions is dependent on the intact immune system and H-FIRE generates 4T1 neoantigens that engage the adaptive immune system to significantly attenuate tumor progression.
Interpretation: Cell death and tumor ablation following H-FIRE treatment activates the local innate immune system, which shifts the tumor microenvironment from an anti-inflammatory state to a pro-inflammatory state. The non-thermal damage to the cancer cells and increased innate immune system stimulation improves antigen presentation, resulting in the engagement of the adaptive immune system and improved systemic anti-tumor immunity.

1. Introduction

Breast cancer is the most common malignancy among women, where almost 1.7 million new patients worldwide are diagnosed annually [1]. When coupled with early detection, current treatments are highly effective and have contributed to a decline in mortality over the last three decades. However, the annual death rate remains

* Corresponding author at: Department of Biomedical Sciences and Pathobiology, Virginia Tech, Virginia Maryland College of Veterinary Medicine, 295 Duckpond Drive, Blacksburg, VA 24061, USA.
E-mail address: icallen@vt.edu (I.C. Allen).

https://doi.org/10.1016/j.ebiom.2019.05.036

Research in context

Evidence before this study

Minimally invasive tumor ablation strategies are being evaluated in a multitude of human cancers. However, studies in breast cancer have been relatively limited thus far. Breast cancer mortality rates remain high and treatments for metastatic disease are inadequate. Likewise, the highly immunosuppressive microenvironment associated with breast cancer is a significant hindrance to emerging immunotherapeutic strategies. Irreversible electroporation (IRE), which utilizes electric pulses to induce cancer cell death through non-thermal mechanisms, is currently being evaluated in preclinical and clinical trials for tumor ablation in a variety of cancers. Intriguingly, several lines of evidence suggest that this technique is effective in immune system activation. Currently, mechanistic insight associated with immune system activation is quite limited.

Added value of this study

In this study, we demonstrate the effectiveness of high-frequency irreversible electroporation (H-FIRE), a novel second-generation modality based on IRE that uses high-frequency bipolar electric pulses instead of unipolar pulses, in mammary tumor ablation. Using a mouse model that closely mimics highly aggressive and metastatic human breast cancer, we show that H-FIRE treatment shifts the local immunosuppressive mammary tumor microenvironment to one that is more pro-inflammatory and facilitates improved adaptive immune system engagement, resulting in the targeting and elimination of metastatic cells.

Implications of all the available evidence

The data presented here suggest that H-FIRE causes localized inflammation through the induction of inflammatory cell death mechanisms and immune cell recruitment. Likewise, H-FIRE improves antigen presentation and promotes systemic anti-tumor immunity. Together, these data suggest that H-FIRE treatment may improve the current standard of care for breast cancer patients and would likely significantly impact the tumor response to immunotherapies or other targeted treatments. H-FIRE may be a valuable tool as a pre-treatment strategy to prime the immune system to eliminate metastases prior to conventional or emerging therapeutic approaches.

unacceptably high. Mortality is typically not associated with breast cancer confined to the breast or draining lymph nodes, rather metastasis to critical organs remains the most significant challenge to patient survival [2].

New therapies for the treatment of breast cancer are emerging including minimally-invasive tumor ablation techniques [3,4]. One particular ablation technology, irreversible electroporation (IRE), has shown promise in both clinical and pre-clinical cancer studies. IRE is a highly innovative locoregional therapy that delivers short unipolar electric pulses that increase the tumor cell transmembrane potential through non-thermal mechanisms, resulting in cell death while sparing critical structures in the treatment field [5]. IRE is currently being evaluated in a range of veterinary and human clinical trials for malignancies in the liver, pancreas, prostate, kidney, and brain [6–16]. However, there are a few disadvantages of IRE including muscle contractions that require medical paralysis for the procedure and a risk of cardiac arrhythmia that requires cardiac synchronization [5]. Due to these limitations, we have developed a novel, next generation technology that utilizes high-frequency bipolar bursts, which minimizes muscle contraction [17] and cardiac arrhythmia risk. This technique is termed high-frequency irreversible electroporation (H-FIRE).

A major advantage of IRE and H-FIRE is immune system engagement through mechanisms that are not yet fully defined [18–22]. Previous work by our team demonstrated that *in vitro* IRE treatment of murine 4T1 mammary cancer cells significantly altered expression of a selection of tumor-associated inflammatory mediators [23]. Likewise, a more recent study utilizing nano-pulse stimulation (NPS), which is similar in principle to IRE and H-FIRE, to treat 4 T1 tumors *in vivo* also demonstrated a reduction in systemic immunosuppressive cells and improved anti-tumor immunity [24]. Similarly, a study showed that electrolytic electroporation invokes an inflammatory response in the liver [21]. Here, we investigate the use of H-FIRE in the mouse 4T1 model of mammary tumorigenesis. We demonstrate that H-FIRE is a highly effective tumor ablation strategy that significantly alters the *in situ* anti-inflammatory tumor microenvironment by stimulating the innate immune system through the induction of inflammatory cell death. Local tumor treatment also results in the activation of the adaptive immune system by improving antigen presentation and reducing local immunosuppressive cell populations. Together, our data show that H-FIRE is effective in the induction of a systemic anti-tumor immune response that is capable of eliminating metastases in locations distal to the primary tumor treatment site.

2. Materials and methods

2.1. H-FIRE treatment parameters

H-FIRE was delivered using a custom bipolar pulse generator (EPULSUS-FBM1-5, Lisboa, Portugal). This generator consists of two unipolar Marx generators capable of producing voltage waveforms with pulse rise-times of 100 ns and a maximum voltage/current output of 5 kV/50 A. For all studies reported here, H-FIRE therapy consisted of applying 200 bursts of bipolar pulses delivered at a frequency of 1 burst per second, where each burst was energized for a total time of 100 μs per burst. Within an individual burst of bipolar pulses, a 2 μs positive pulse, 5 μs inter-pulse delay, 2 μs negative pulse, and a 5 μs inter-pulse delay (2-5-2) pattern was repeated until a total on-time of 100 μs per H-FIRE burst was achieved (waveforms are shown in Supplemental Fig. S1A—B). While several voltage-to-distance ratios were applied for both *in vitro* and *in vivo* experiments, all other H-FIRE pulsing parameters in this study were conserved.

2.2. In Vitro 4T1 H-FIRE treatment parameters

The murine 4T1 mammary tumor cell line was acquired from ATCC (Cat#CRL-2539). Cells were sub-cultured to approximately 80% confluence. All experiments were performed within the first 4–8 sub-cultures. At confluence, 4T1 cells were washed and resuspended in a 5.5:1 ratio of low-conductivity sucrose solution (85 g sucrose, 3.0 g glucose, 7.25 ml RPMI, and 992.75 ml DI water) to unsupplemented RPMI to 4×10^6 cells/ml. An 800 μl cell suspension was added to a 4 mm sterile electroporation cuvette (Fisher Scientific) and H-FIRE was delivered at a voltage of 204 V, 800 V, or 1600 V totaling 500, 2000, or 4000 V/cm electric field magnitude, respectively. Temperature was monitored by inserting a fiber optic temperature probe (Lumasense, Inc.) within the cuvette during pulsing. Shortly after pulsing ceased, the temperature probe was removed and the cells were maintained on ice. Aliquots were immediately removed for staining with acridine orange (AO)/propidium iodide (PI) for automated cell viability counting using a Cellometer Vision CBA Image Cytometer (Nexcelom) and trypan blue for manual cell viability counting *via* hemocytometer. Remaining cells were divided and plated at a density of approximately 600,000 cells/ml, and maintained in incubators for either 2, 8, or 24 h before

supernatant was isolated for LDH Cytotoxicity Assay (Pierce) following manufacturer's protocol.

2.3. Experimental animals

All experiments were conducted under institutional IACUC approval and in accordance with the NIH Guide for the Care and Use of Laboratory Animals. All experiments utilized 6–10 week-old, female BALB/cJ (n = 3–10 animals in each group) or NOD scid gamma (NSG) (n = 3–10 animals in each group) mice (Jackson Labs). 4 T1 cells were washed and re-suspended in sterile PBS prior to injection. Mice were anesthetized and 1.2×10^6 cells were injected into the mammary fat pad. Clinical parameters and tumor measurements were evaluated at least three times/week. Tumor diameter was calculated by the square root of the product of two perpendicular diameters, as previously described [25]. Animals were euthanized when tumors reached 1.6 cm of calculated diameter, or if considered clinically moribund. All studies were repeated at least 3 individual times to ensure reproducibility.

2.4. In Vivo H-FIRE tumor treatment

On days 10–11, mice were anesthetized using isoflurane and two needle acupuncture electrodes with 0.4 mm diameter were inserted into the tumor. H-FIRE was applied with a voltage to distance ratio of 2500 V/cm and the electrode separation was set to match tumor diameter using one of the following 3 combinations: 3 mm spacing/750 V; 5 mm spacing/1250 V; or 6 mm spacing/1500 V, ensuring a 2500 V/cm voltage-to-distance ratio was administered to each tumor. Electrode spacing was calculated as the distance between the centers of the two electrodes. Mice were recovered on room air.

2.5. Tissue collection and processing

At euthanasia, the primary tumor was dissected, half was flash frozen for RNA isolation, half was fixed in formalin for histopathology. Whole blood was collected *via* cardiac puncture, washed in HBSS, and resuspended in IMDM supplemented with 10% FBS, 100 units/ml penicillin, 100 μg/ml streptomycin, and 60 μM 6-thioguanine. After 7–12 days incubation, media was removed from the plates, cells were fixed in methanol, stained with 0.03% methylene blue, and counted. The large lobe of the lung was isolated, inflated with formalin, and prepared for histopathology.

2.6. Histopathology

Paraffin-embedded formalin-fixed tissues were stained with H&E and independently evaluated by blinded board-certified veterinary pathologists (S.C.O. & K.E.). Pulmonary metastases were quantified per section. Tumor necrosis was graded as a percentage: 0, 0% necrosis; 1, 1–25% necrosis; 2, 26–50% necrosis; 3, 51–75% necrosis; 4, 76–100% necrosis. Tumor leukocyte infiltration was scored on a scale of low, moderate, or high. The skin surrounding the tumor was graded using a binary score for detection of fibrosis.

2.7. Flow cytometry

Tumors were isolated from the animals and mechanically digested. Cells were diluted in complete RPMI. For cell surface marker staining, after an initial 30-min incubation with anti-CD16/32 (Fc block) in FACS buffer at 4 °C, cells were stained for 30 min in the dark at 4 °C. Cells were washed with PBS and evaluated by FACSAria (BDBiosciences). The same protocol was followed for surface marker staining, followed by permeabilization with True-Nuclear™ Transcription Factor Buffer Set (BioLegend) following the manufacturer's guidelines for use with FOXP3 staining.

2.8. Gene expression profiling and pathway analysis

For *in vivo* studies, total RNA was harvested from primary tumors using FastRNA Pro Green Kit following manufacturer's protocols (MP Biomedicals). Total RNA was pooled from 3 to 8 individual mice per group for RT^2 Profiler PCR Array Platform (QIAgen) cDNA reaction. For *in vitro* experiments, total RNA was harvested using TRIzol (Invitrogen). Total RNA was pooled from 8 to 9 samples per treatment for the cDNA reaction. Gene expression was evaluated using PAMM-131Z and PAMM-181Z arrays (*in vivo*), or PAMM-052Z (*in vitro*)(Qiagen) following manufacturer's protocols. The gene list for each array and functional categories for each gene are available through the manufacturer. Ingenuity Pathways Analysis (IPA) and the manufacturer's array software (Qiagen) was used to analyze gene expression data. IPA data were ranked and evaluated based on z-score.

2.9. Replicates

All studies were repeated at least 3 independent times unless noted.

2.10. Statistical analysis

Data were analyzed using GraphPad Prism, version 7. A Student's two-tailed *t*-test was utilized for comparisons between two experimental groups. Multiple comparisons were conducted using one-way and two-way ANOVA where appropriate followed by Mann-Whitney or Tukey post-test for multiple pairwise examinations. Statistical significance was defined as $p \leq 0.05$. All data are represented as the mean ± SEM.

3. Results

3.1. H-FIRE is capable of delivering high voltages with minimal changes in temperature

Our team previously defined unipolar IRE pulse parameters that were highly effective in promoting cell death and altering expression of mediators associated with immune system activation in 4T1 cells *in vitro* [23]. Using these studies as our reference, we sought to evaluate similar parameters for H-FIRE in 4 T1 cells. 4 T1 cell suspensions were exposed to H-FIRE with electric field strengths of 0, 500, 2000, and 4000 V/cm while suspended in a cuvette at room temperature (Fig. 1A) and Joule heating was monitored throughout the duration of treatment. A significant increase in temperature was observed at 4000 V/cm, with maximum temperature reaching 62 °C, whereas the maximum temperature was 28.6 °C at 2000 V/cm (Fig. 1B). The maximum temperature change for the two lower electric field magnitudes remained below 37 °C. To detect cell viability, both manual trypan blue and automated AO/PI live/dead exclusion staining was recorded immediately following H-FIRE treatment at each voltage (Fig. 1C). At 2000 V/cm, we observed a 29% decrease in cell viability immediately after treatment (Fig. 1C). In order to determine whether cell death was maintained over time following H-FIRE, we chose to use an LDH assay following 2000 V/cm treatment (Fig. 1C). Here, we show steady and consistent cell death beginning within 2 h post-treatment and lasting over a 24-h time course (Fig. 1C). This is consistent with the unique cell death mechanisms driven by electroporation-based ablation therapy that are time-dependent, with cell death detectable up to a week after treatment [26]. Unlike other forms of non-thermal tumor ablation, such as histotripsy that causes instant cell rupture [27], the cell death induced by H-FIRE continues over an extended timeframe.

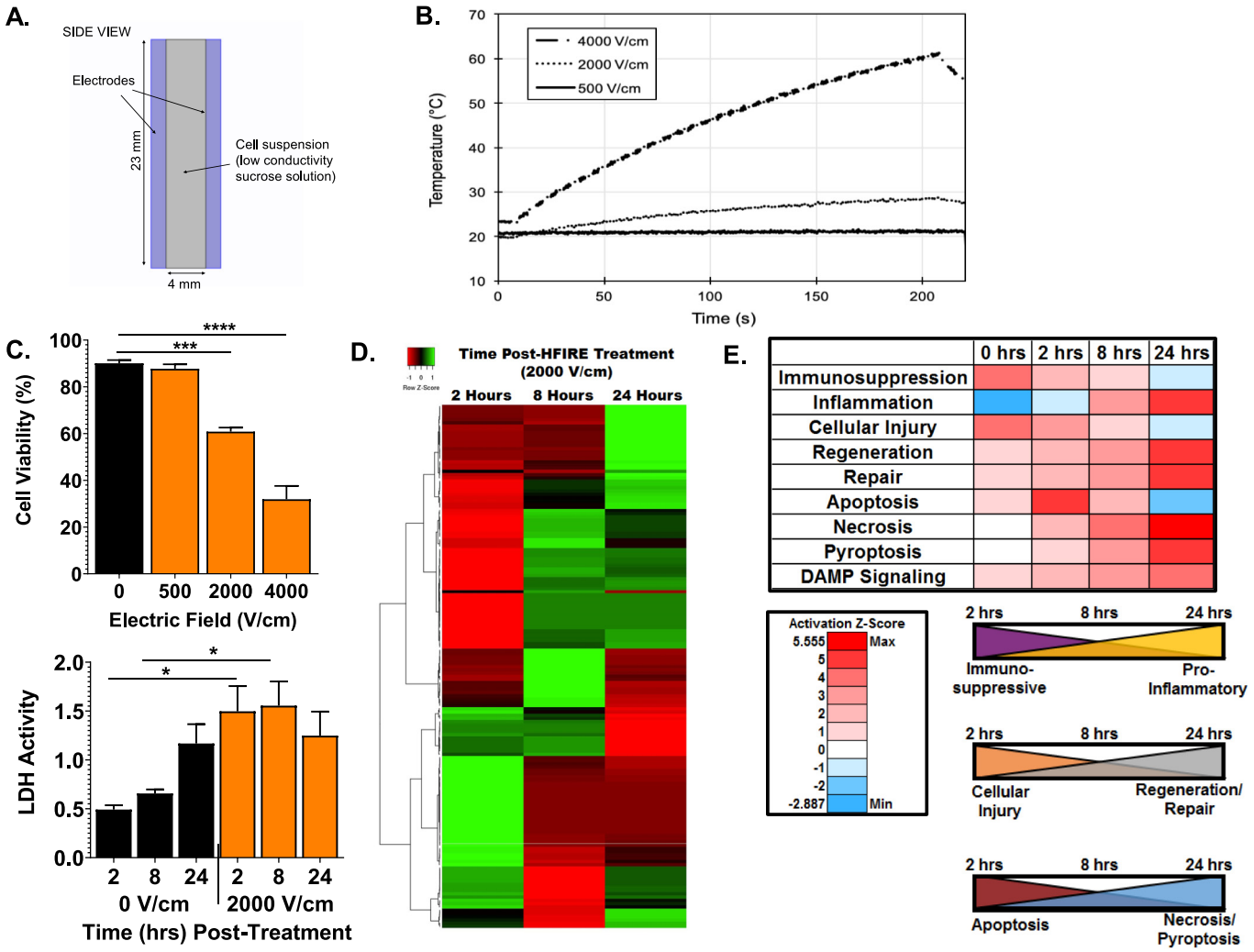
A.
SIDE VIEW
Electrodes
23 mm
Cell suspension
(low conductivity
sucrose solution)
4 mm
B.
4000 V/cm
2000 V/cm
500 V/cm
Temperature (°C)
Time (s)
C.
Cell Viability (%)
Electric Field (V/cm)
LDH Activity
0 V/cm
2000 V/cm
Time (hrs) Post-Treatment
D.
Time Post-HFIRE Treatment
(2000 V/cm)
2 Hours
8 Hours
24 Hours
E.
0 hrs
2 hrs
8 hrs
24 hrs
Immunosuppression
Inflammation
Cellular Injury
Regeneration
Repair
Apoptosis
Necrosis
Pyroptosis
DAMP Signaling
Activation Z-Score
Max
Min
Immuno-suppressive
Pro-Inflammatory
Cellular Injury
Regeneration/ Repair
Apoptosis
Necrosis/ Pyroptosis
F.
z-score = 0.689
z-score = 0.000
z-score = 2.922
z-score = 3.326
Pycard
G.
Reactive Oxygen Species
ATP
HMGB1

3.2. H-FIRE promotes inflammatory cell death and attenuates local 4T1 tumor-promoting microenvironments

IRE treatment of 4 T1 cells results in up-regulation of IL-6 and TNF, and down-regulation of TSLP [23]. To better define the impact of H-FIRE on 4 T1 cells, we utilized a broader gene expression profiling strategy coupled with Ingenuity Pathway Analysis (IPA) to profile changes for 162 genes associated with cancer hallmarks and inflammation (Supplemental Table S1A). For this study, we utilized 4 T1 cells treated with 2000 V/cm and tracked gene expression changes over 2, 8, and 24-h (Fig. 1D-E). IPA identified several disease and biological functions impacted by H-FIRE treatment based on the expression profiles (Supplemental Fig. S2A). Likewise, we observed differential effects on a range of genes and networks following 4 T1 cell treatment (Fig. 1D; Supplemental Fig. S2B). Using these data and IPA, we were able to group the gene expression profiling changes into 9 specific pathways related to 3 biological functions that were differentially impacted by H-FIRE treatment over time (Fig. 1E). H-FIRE treatment resulted in significant changes in pathways associated with inflammation, cellular injury/repair, and cell death (Fig. 1E). Specifically, H-FIRE induced robust down-regulation of genes associated with immunosuppression and reciprocal increases in pro-inflammatory genes (Fig. 1E). We also observed significant decreases in genes associated with cellular injury and an increase in genes associated with regeneration and repair (Fig. 1E). This is potentially associated with cells beginning to recover from electroporation.

Consistent with viability studies, we also observed significant increases in expression profiles associated with cell death pathways (Fig. 1E). Specifically, we observed a significant increase in pathways associated with inflammatory cell death signaling and necrosis over the 24-h time course (Fig. 1E). Prior studies of IRE have suggested that cell death occurs through apoptosis [28–31]. Interestingly, we do observe a gene expression profile that is consistent with apoptosis shortly after H-FIRE (Fig. 1E). However, this appears to shift over time towards inflammatory cell death and necrosis (Fig. 1E). By 24 h, we observed up-regulation of genes and pathways associated with necrosis and pyroptosis, which are inflammatory forms of cell death associated with NLR inflammasome and caspase-1/11 activation (Fig. 1F). IPA identified significant changes in genes and networks associated with *Pycard* signaling following H-FIRE treatment (Fig. 1F, box). *Pycard* encodes the essential inflammasome adaptor-protein ASC, critical for inflammation and pyroptosis. Pyroptosis is associated with pattern recognition receptor recognition of damage associated molecular patterns (DAMPs) following pathogen exposure, cellular damage, or stress [32]. Further evaluation of the gene expression data revealed 3 networks associated with DAMP signaling significantly up-regulated post-H-FIRE: (1) ROS signaling, (2) ATP signaling, and (3) high mobility group box 1 (HMGB1) signaling (Fig. 1G), which are also associated with NLR inflammasome activation and previously shown to be inducers of pyroptosis [33–35].

3.3. H-FIRE is a highly effective ablation therapy in the In Vivo 4T1 mammary tumor model

To better define the effectiveness of H-FIRE in mammary tumors, we utilized the *in vivo* murine 4T1 mammary carcinoma model [25]. Animals were injected with 1.2×10^6 4T1 cells into a single mammary fat pad. We chose to treat the tumors when they reached ~5 mm in diameter, which occurs between days 10–11 of our model (Fig. 2). Each tumor received 2500 V/cm H-FIRE treatment. The schematic illustrates a pair of 0.4 mm electrodes, spaced 3–6 mm apart to deliver H-FIRE (Fig. 2A). The 2500 V/cm H-FIRE treatment was sufficient to ablate the 4T1 mammary tumor (Fig. 2B). Representative images of mice showing average tumor sizes on Day 15 (4 days post-treatment) revealed an average 80% reduced tumor diameter post-H-FIRE (Fig. 2C). The only H-FIRE side effect noted was superficial scab formation over the treatment area, which resolved within 2 weeks post-treatment (Fig. 2C; Supplemental Fig. S3C-E). Similar scabbing was not observed in mice treated with H-FIRE that were not tumor-bearing (Fig. 2C; Supplemental Fig. S3C-E). We achieved near-full ablation within the first week following treatment. However, we observed a range of tumor responses to treatment by day 27 with some tumors beginning to regrow (Fig. 2B).

We believe the ability to administer H-FIRE without the muscle contraction side effects is a major clinical advantage of this technology over other electroporation approaches. Thus, here we compared muscle constriction associated with the current standard monopolar IRE pulse *versus* the bipolar H-FIRE burst for the same pulse amplitude. Animals were fitted with accelerometers on their footpads and contraction was assessed during 2000 V/cm of either IRE or H-FIRE. IRE treatment resulted in significant full body muscle spasm (Fig. 2D; Supplemental Video S1; Supplemental Fig. S3A; partial treatment shown for clarity), while negligible movement was observed during H-FIRE treatment (Fig. 2E; Supplemental Video S2; Supplemental Fig. S3B; partial treatment shown for clarity). Together, these data show that H-FIRE effectively ablates the 4T1 orthotopic tumor and can be applied without the muscle contraction side effects associated with IRE for the same electric field magnitude. However, it should be noted that H-FIRE treatments require a higher applied pulse amplitude in order to achieve an equivalent lesion depending on the pulse width [36,37]. Sano et al. demonstrated *in vitro* ablations with H-FIRE (pulse width 2 μs) *versus* IRE (pulse width 100 μs) required 1.5 times higher electric fields for similar lesions; whereas, Mercadal et al. show the stimulation threshold for H-FIRE *versus* monopolar IRE were >1 order of magnitude larger, suggesting that this tradeoff is worthwhile [17,36,38]. Though not the focus of this study, we show here that muscle excitation with H-FIRE is mitigated, further supporting previous numerical modeling efforts of Mercadal et al. [38].

3.4. H-FIRE ablation results in increased cell death and inflammation

To determine the extent and mechanisms of mammary tumor ablation following H-FIRE, cell death and inflammation within the tumor were evaluated by histopathology. The 4T1 mammary tumor demonstrates many features of aggressive breast cancer including severe dysplasia, invasive behavior, marked anisocytosis and anisokaryosis, multinucleated cell formation, and high mitotic index (Fig. 3A). Previous studies have shown that these tumors characteristically have high levels of necrosis in their core regions and significant 4T1 cell proliferation in the leading edge of the tumor [25]. These tumors are also highly immunosuppressive with low levels of lymphocyte infiltration in the microenvironment [25]. Our histopathology assessments are consistent with this and revealed large areas of cell death in the central core of the

Fig. 1. High Frequency Irreversible Electroporation (H-FIRE) Induces Inflammatory Cell Death and Effectively Attenuates the Tumor Promoting Microenvironment *In Vitro*. A total of 200H-FIRE waveforms were delivered once per second with a uniform voltage of either 240 V, 800 V, or 1600 V across the 4 mm cuvette totaling 500, 2000, or 4000 V/cm, respectively. A. Schematic of H-FIRE delivery to 4 T1 cells in a 4 mm cuvette. B. Temperature during *in vitro* H-FIRE treatment. At 2000 V/cm, cell suspension temperature remains below 30 °C. C. Influence of electric pulse parameters on cell viability. Cell viability was determined *via* trypan blue (manual) and AO/PI staining (automated); the average percent viability shown. LDH Activity was utilized to evaluate cell death at 2000 V/cm over time. D-H. Real time PCR-based gene expression arrays were utilized to evaluate the expression of 162 genes associated with cancer and inflammation. D. Heat map of gene expression changes at 2, 8, and 24 h following H-FIRE treatment with 2000 V/cm. E. Ingenuity Pathway Analysis (IPA) of gene expression data revealed significant shifts in pathways associated with inflammation, injury/repair, and cell death. F. Gene expression analysis further indicates that necrosis and pyroptosis are the dominant forms of cell death 24 h post-H-FIRE treatment. The z-score reflects the activation of the pathway at the time point shown. G. IPA identified significant changes in pathways associated with reactive oxygen species, adenosine triphosphate, and HMGB1 signaling. All studies were repeated at least 3 times. $^{*}p < 0.05$; $^{***}p \leq 0.001$.

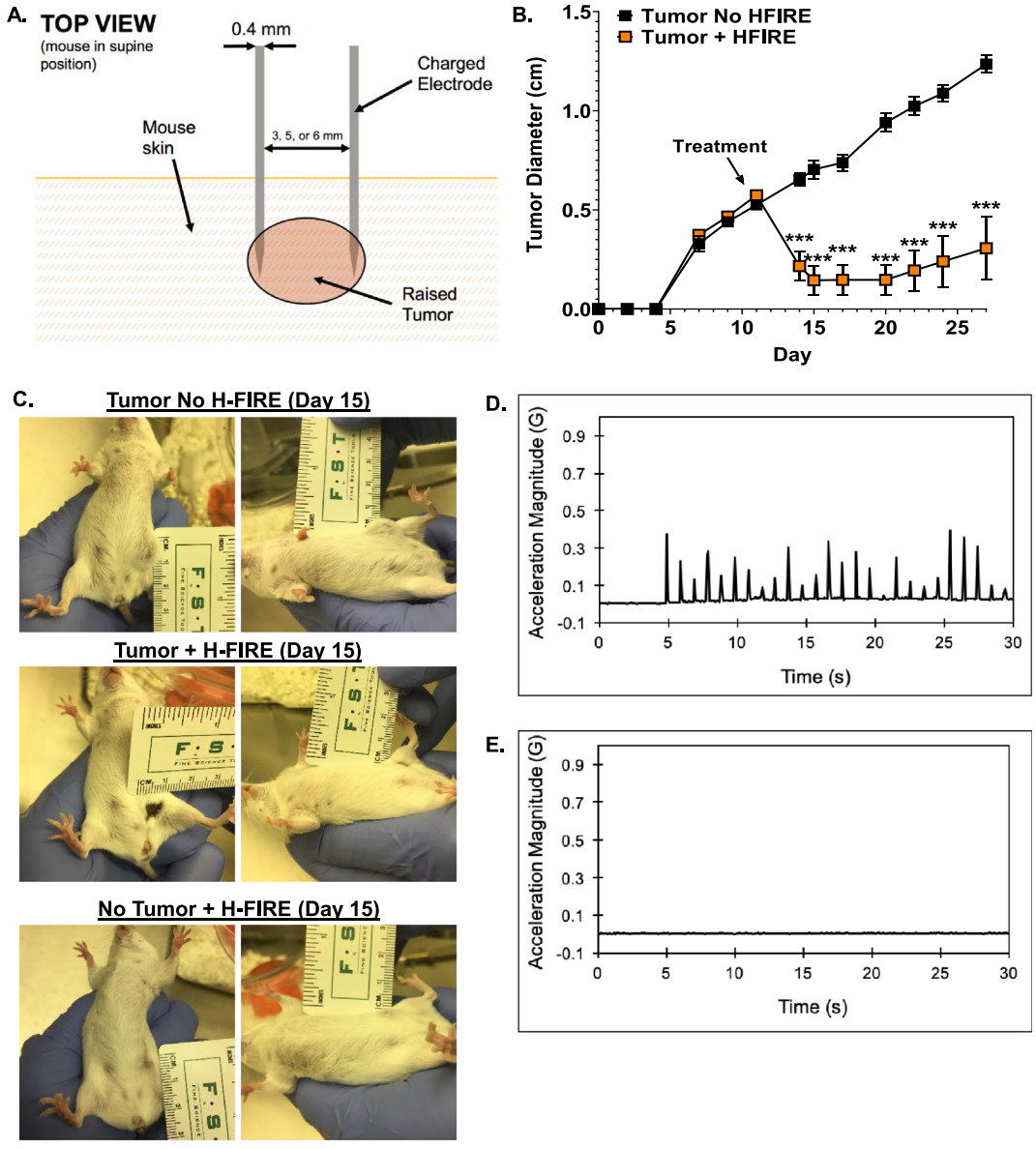

Fig. 2. H-FIRE Treatment Results in Significant Tumor Ablation in the *In Vivo* 4 T1 Mammary Tumor Model. Mice were injected with 1.2×10^6 4 T1 cells into the mammary fat pad of wild type BALB/c mice. On day 11, mice were anesthetized and needle electrodes were inserted into the tumor to deliver 200H-FIRE waveforms once per second at 2500 V/cm (voltage-to-distance ratio). Animals were monitored a least 3 times/week for clinical parameters and tumor progression. A. Schematic illustrating treatment strategy and electrode placement. B. Tumor diameter changes following H-FIRE reveals significant decreases in tumor diameter and progression. C. Images of tumors from representative animals 15 days post-H-FIRE treatment. 4 T1 tumor/H-FIRE sham treatment (top panels); 4 T1 tumors and H-FIRE treatment (middle panels); no tumor/no H-FIRE treatment (bottom panels). D. A zoomed-in plot of accelerometer output at 2000 V/cm (voltage-to-distance ratio) IRE. E. A zoomed-in plot of accelerometer output at 2000 V/cm (voltage-to-distance ratio) H-FIRE. $n = 3$–10 mice in each experimental group. $^{***}p \leq 0.001$.

4T1 mammary tumors (Fig. 3B). Following H-FIRE, we routinely observed expanded areas of cell death and tumor cell ablation (Fig. 3C). By the end of the 30 day 4T1 animal model, no histopathological signs of tumor were detected during pathological assessments of the mammary fat pad in 30% of H-FIRE-treated animals (Fig. 3D). Consistent with the *in vitro* data, H-FIRE induced a gene expression profile consistent with necrosis and pyroptosis rather than apoptosis (Fig. 3D; Supplemental Fig. S1B). Because necrosis and pyroptosis are inflammatory forms of cell death, we next evaluated histopathologic features of inflammation. Following H-FIRE treatment, we observed increases in immune cell infiltration into the treatment zone (Fig. 3F-H). However, our histopathology assessments revealed that immune cell infiltration was variable between animals and ranged from none to moderate following H-FIRE treatment (Fig. 3F-H). Together, these data support a proposed mechanism whereby H-FIRE alters the tumor microenvironment through the induction of inflammatory cell death, either necrosis or pyroptosis.

3.5. Tumor response to H-FIRE ablation is correlated with increased cellular immunity

Based on the range of ablation responses to H-FIRE, we sought to characterize the microenvironment in animals sub-classified as low-, average-, or high-responders to treatment. It is important to note that all of the tumors demonstrated significant ablation by volume following H-FIRE, ranging from 68 to 100% ablation. At necropsy, 15 days post-H-FIRE, tumor specimens were collected and RNA was extracted; data were analyzed based on percentage of ablation post-H-FIRE (low response 68–84% ablation; average response = 85–94% ablation; high response ≥95–100% ablation). When animals were sub-grouped based

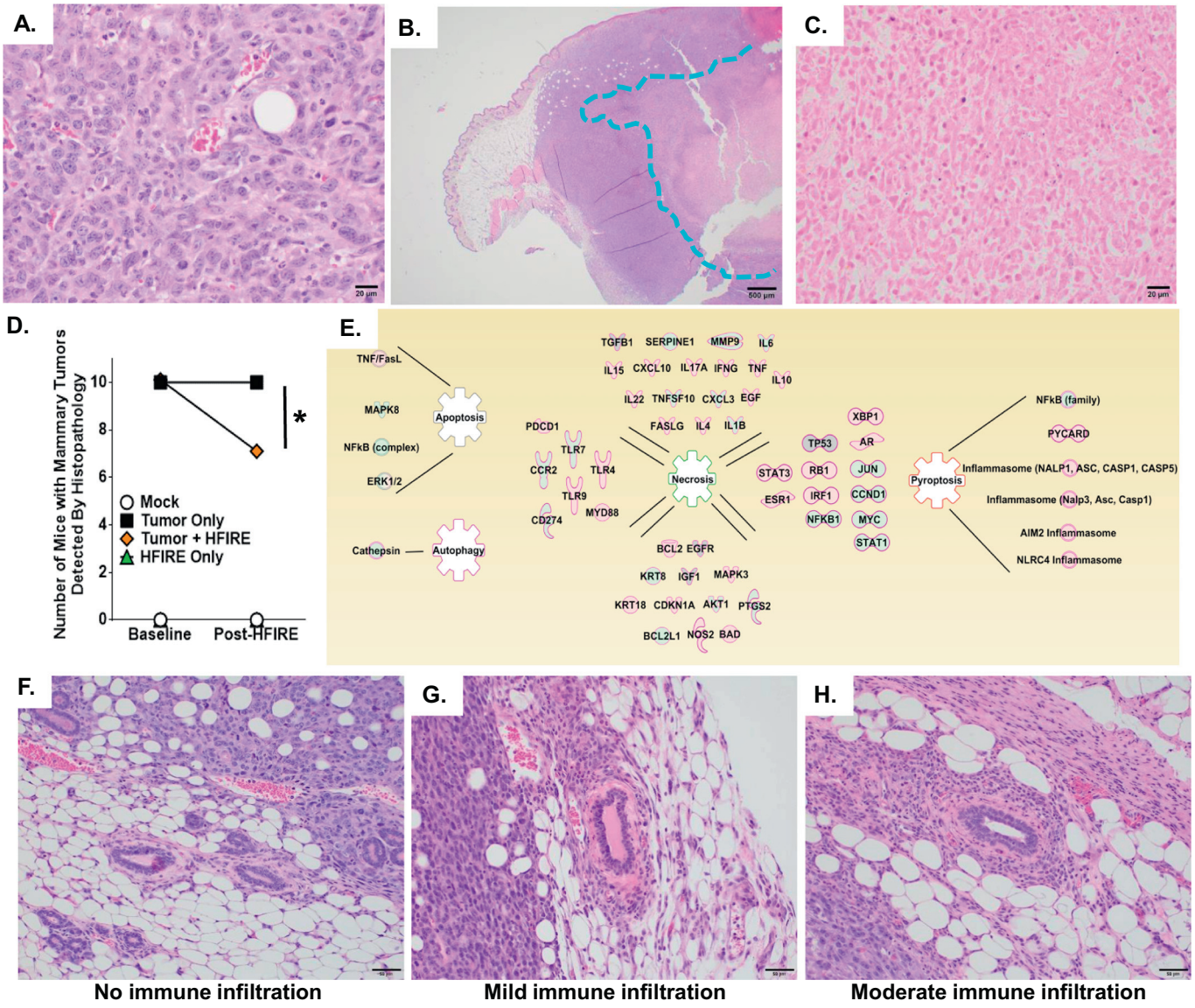

Fig. 3. H-FIRE Ablation Results in Significant Cell Death and Inflammation. Histopathology evaluation revealed significant signs of cell death in the 4T1 mammary tumor that was increased following H-FIRE. A. The architecture of the untreated 4T1 tumors remains intact, with aggressively proliferating neoplastic cells obliterating normal subcutaneous structures. B. The central core of these large tumors often contains abundant necrosis, and can be visually distinguished from the rest of the neoplasm (blue line). C. Following H-FIRE application, neoplastic cells in the treatment zone undergo cell death as evidenced by nuclear pyknosis and loss, cytoplasmic blanching, and disintegration of cellular architecture. D. Pathology assessments of the H-FIRE treated areas revealed a significant decrease in histologically identifiable mammary tumors. E. Gene expression arrays were utilized to evaluate 156 genes associated with cancer and inflammation. IPA analysis revealed that necrosis and pyroptosis are significantly increased and are the dominant pathways associated with cell death following H-FIRE treatment compared to the untreated 4T1 tumors *in vivo*. F. Typical 4T1 tumors are relatively immunosuppressive with minimal immune cell infiltration. G-H. Following H-FIRE, histopathology revealed increased inflammation. This inflammation could be further sub-classified as either (G) mild or (H) moderate. n = 3–10 mice in each group. $^{*}p \leq 0.05$.

on their individual tumor response to H-FIRE, we observed a significant correlation between tumor response and expression of genes associated with cellular immunity (Fig. 4A). In mice with low response to H-FIRE, the majority of genes associated with cellular immunity were significantly decreased (Fig. 4A). Correlation analysis revealed a strong positive correlation ($r = 0.70$) between up-regulation of cellular immunity-associated genes and decreased tumor diameter. The biggest shifts in individual gene expression were noted for *Aicda*, *Ccl20*, *Ccl28*, and *Fasl*, which were significantly down-regulated in low-responding tumors and significantly up-regulated in highly responsive tumors (Fig. 4A). Analysis of cellular immunity networks most impacted by H-FIRE treatment revealed significant differences in chemokine signaling (Fig. 4B). The majority of chemokine-associated gene expression was down-regulated in untreated tumors, with notable exceptions being *Ccr1*, *Ccr2*, *Ccr5*, and *Cxcl6* up-regulated (Fig. 4B). However, this pattern was reversed in H-FIRE-treated tumors where we observed significant down-regulation of these genes and the vast majority of remaining genes in this network significantly up-regulated (Fig. 4B). Together, these data suggest that activation of cellular immunity is associated with the effectiveness of H-FIRE ablation and chemokine signaling networks play a critical role in optimal responses to treatment.

To further evaluate H-FIRE-mediated changes in the *in situ* 4T1 tumor microenvironment, we utilized IPA to identify biological functions and gene networks impacted by treatment. We observed significant down-regulation of breast cancer-associated genes, with lower levels of expression observed in fully ablated tumors compared to the low-responder and untreated tumor groups (Fig. 4C). Similar to our findings in the *in vitro* studies, we observed a significant shift in the balance between immunosuppressive and pro-inflammatory-associated gene transcription (Fig. 4C). Following treatment, gene expression

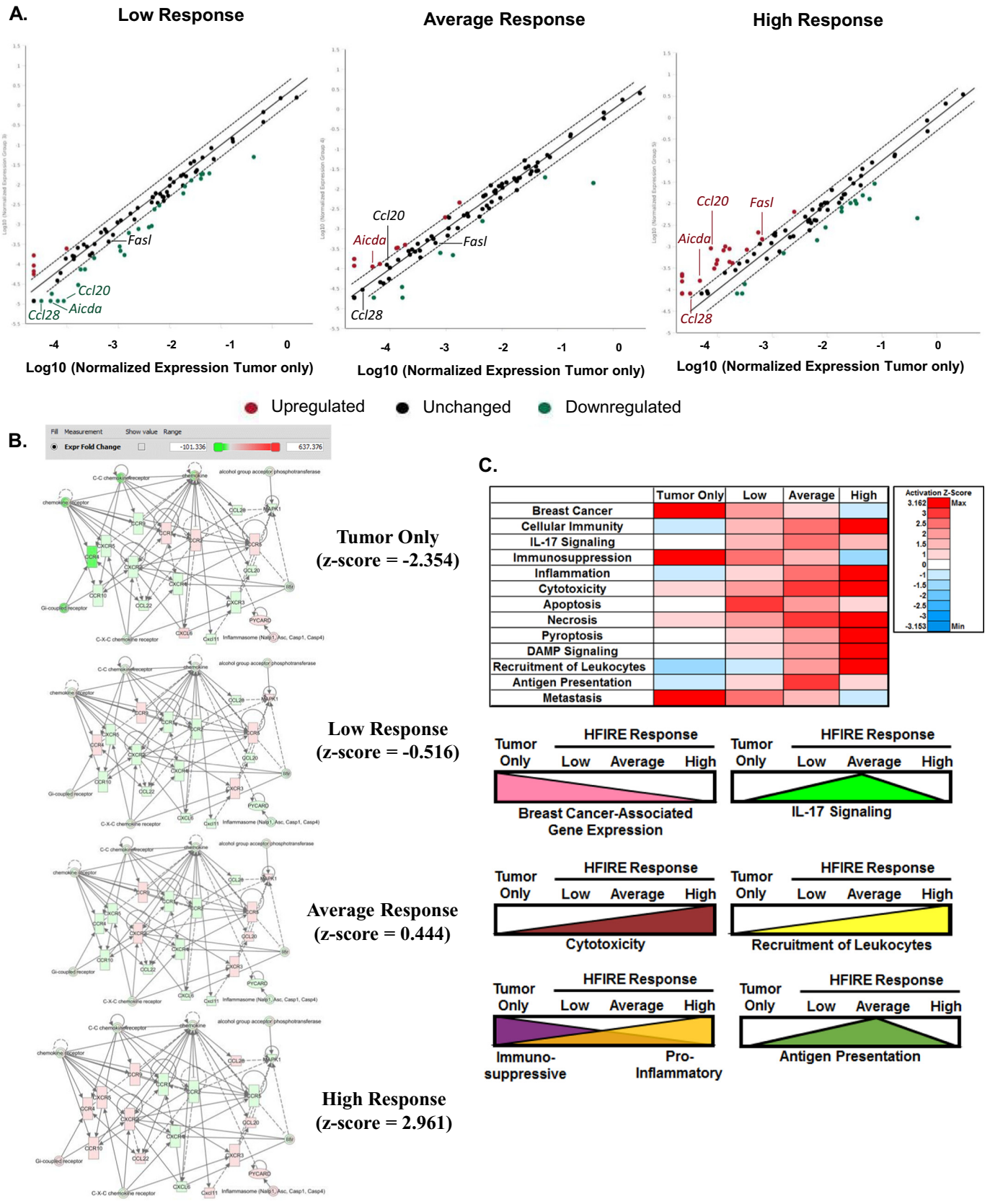

profiles associated with immunosuppression were significantly down-regulated, while genes associated with inflammation and pro-inflammatory immune responses were significantly up-regulated (Fig. 4C). These responses were increased in average- and high-responder groups, compared to the low-responders and untreated animals (Fig. 4C). Signaling networks associated with cytotoxicity were significantly increased in responsive tumors (Fig. 4C), likely associated with increased cell death following treatment. Consistent with the chemokine data (Fig. 4B), gene networks associated with recruitment of leukocytes were significantly up-regulated in responsive

tumors (Fig. 4C). Interestingly, IL-17 signaling and antigen presentation networks were up-regulated in average-responder animals compared to the other sub-groups (Fig. 4C). We are unsure of the functional significance of the IL-17 findings as this cytokine has been shown to have both pro- and anti-tumor effects in breast cancer, including increased recruitment of tumor-associated neutrophils and promoting cytotoxic T cell responses [39,40]. However, the data associated with increased antigen presentation signaling is consistent with the pro-inflammatory shift observed in the tumor microenvironment and may suggest that adaptive immune system signaling may benefit from a partial or an incomplete tumor ablation strategy. Together, the data presented here are consistent with those described for the *in vitro* studies and detail the tumor microenvironment shifts from one that is favorable for tumor progression to an antitumor microenvironment driven by increased cellular immunity.

3.6. H-FIRE treatment significantly alters local immune cell populations in 4T1 tumor microenvironment

Based on the clinical findings and expression profiling data, we next sought to define the impact of H-FIRE on cell populations within the tumor microenvironment to identify mechanism/s associated with increased cellular immunity. Similar to most human breast cancers, the 4 T1 microenvironment is characterized as being highly immunosuppressive [25]. While many factors contribute, the recruitment and assimilation of myeloid derived suppressor cells (MDSCs), regulatory T cells (Tregs), tumor-associated macrophages (TAMs), and tumor associated neutrophils (TANs) are potent factors in thwarting anti-tumor immunity [41]. Because these cells are in and around the H-FIRE treatment zone and previous studies have shown that IRE and nanopulse treatments can impact these populations [24,42], we evaluated these cells post-treatment using flow cytometry. Tumors were harvested during necropsy two and seven days post-H-FIRE treatment and digested to generate single cell suspensions for labeling and analysis. Common markers were utilized to identify neutrophils, polymorphonuclear-MDSCs (pMDSCs), monocytic-MDSCs (mMDSCs), TAMs, Tregs, and T helper cell populations (Supplemental Fig. S4A). Two days after H-FIRE treatment, we observed an 8.7% decrease in CD11b + Ly6G+ neutrophils and no CD11b + Ly6G + Ly6C^{lo}CD45- pMDSCs in the H-FIRE-treated animals (Fig. 5A). Although there were trending differences in these populations seven days post-H-FIRE, no significant differences were observed at this later time point (Supplemental Fig. S4B). We detected a significant 12.5% decrease in CD4 + CD45+ T helper cell populations two days after treatment (Fig. 5B). Somewhat counterintuitively, we saw a small but significant increase (0.15%) in the CD4 + CD45 + CD25^{hi}CD127^{lo}Foxp3+ Treg population (Fig. 5B). No significant differences were observed in these lymphocyte populations after seven days (Supplemental Fig. S4C). Regarding TAM populations, no significant differences were observed two days after treatment (Supplemental Fig. S4D). However, this may suggest the macrophage populations in the treatment zone are resistant to initial death by H-FIRE because at seven days, we observed a significant decrease in CD11b + Ly6G-Ly6C-CD45 + F4/80+ TAMs (Fig. 5C). The reduction in TAN, MDSC, and TAM populations and the congruent attenuation of their anti-inflammatory signaling is consistent with the shift to a pro-inflammatory anti-tumor microenvironment observed following H-FIRE.

3.7. Local H-FIRE treatment promotes a systemic anti-tumor immune response

Due to the increase in cellular immunity signaling, we hypothesized we would observe increased adaptive immune system activation. Animals were necropsied 15 days post-H-FIRE, and lungs and blood were evaluated for metastatic lesions. Pulmonary metastatic lesions were characterized using blinded histopathology examination (Fig. 6A). We observed 46.7% reduction in the number of lung lesions counted post-H-FIRE (mean = 8.367 ± 1.731) compared to untreated animals (mean = 15.03 ± 2.392) (Fig. 6B). IPA expression profiling revealed a significant decrease in metastasis-associated genes in the primary tumor post-H-FIRE (Fig. 6C). The extent of down-regulation was consistent with the response to H-FIRE, with the greatest changes in average- or high-responders (Fig. 6C). Thus, it is possible that the changes in lung metastases were a direct reflection of the level of tumor ablation and down-regulation of metastatic genes in the primary tumor. However, it should be noted that we did not detect a significant correlation between the numbers of actual pulmonary metastatic lesions and the response to treatment. Rather, our data shows a significant decrease in metastasis when all of the treated animals are grouped together and compared against untreated mice. It is also probable that metastasis was already underway at the time of treatment in this model. Thus, it is also likely that local ablation with H-FIRE effectively activated systemic anti-tumor immunity, resulting in the observed reduction in the metastatic tumor burden.

To evaluate the role of the immune system in controlling metastasis following H-FIRE, we utilized NSG mice that lack T, B, and NK cells. Animals were injected with 1.2×10^6 4T1 cells in the mammary fat pad and treated with identical H-FIRE parameters as wild type BALB/c animals when tumors reached 0.5–0.6 cm (Fig. 6D). We observed significant ablation in the 4T1 tumors with average diameter decreasing from 0.56 cm to 0.30 cm post-H-FIRE (Fig. 6D). While this decrease was statistically significant compared to untreated NSG animals, tumor diameter remained larger than those of wild type BALB/c mice post-treatment, ablation demonstrated greater variability, and no tumors were completely ablated (Fig. 6D). Likewise, the level of ablation steadily decreased until the tumor reached the original size at treatment (0.57 cm) by Day 25 (Fig. 6D). In both the untreated and H-FIRE-treated NSG animals, we observed high numbers of metastatic cells in the blood (Fig. 6E). In the untreated animals, we counted 4994 ± 2786 colonies and 6806 ± 2842 colonies in H-FIRE-treated NSG animals (Fig. 6E). In BALB/c mice we counted 2401 ± 503.7 colonies in the blood from untreated mice and 853.2 ± 437.7 colonies in H-FIRE-treated animals (Fig. 6E). The significant decrease in circulating metastatic 4T1 cells following local H-FIRE treatment of the primary tumor was statistically significant and based on the NSG experiment is dependent on an intact immune system.

3.8. H-FIRE ablation generates Neoantigens capable of stimulating the adaptive immune system

While the innate immune system and cellular immunity contribute to tumor ablation, initiation of systemic anti-tumor immunity relies on robust adaptive immune system activation, largely driven by tumor antigen presentation at the local treatment site. Based on our data, we

Fig. 4. Tumor Response to H-FIRE Ablation is Correlated with Increased Cellular Immunity. At necropsy 15 days post H-FIRE, tumor specimens were collected and total RNA was extracted for gene expression profiling. Data were analyzed based on the % of tumor ablation following H-FIRE (low response≤85% ablation; average response = 85%–94% ablation; high response≥95% ablation). A. The up-regulation of genes associated with cellular immunity are strongly correlated with tumor ablation. In tumors classified in the low-responder group, a significant number of genes associated with cellular immunity were down-regulated. Conversely, a significant number of genes were up-regulated in the animals that saw the highest levels of tumor ablation. B. Chemokine signaling networks were the most impacted by H-FIRE treatment, with highly responsive tumors demonstrating a significant up-regulation compared to the other groups. The z-scores shown reflect the level of signaling pathway activation between each group. C. Further pathway analysis identified 6 additional signaling networks that were significantly impacted by H-FIRE treatment response. We observed a significant decrease in breast cancer-associated gene expression and immunosuppression from untreated to high therapeutic response. Conversely, we observed a significant increase in gene expression associated with inflammation, cytotoxicity, and recruitment of leukocytes over the same treatment scale. We also observed a significant increase in IL-17 signaling and antigen presentation that was highest in the animals with average responses. $n = 3$–10 mice in each group.

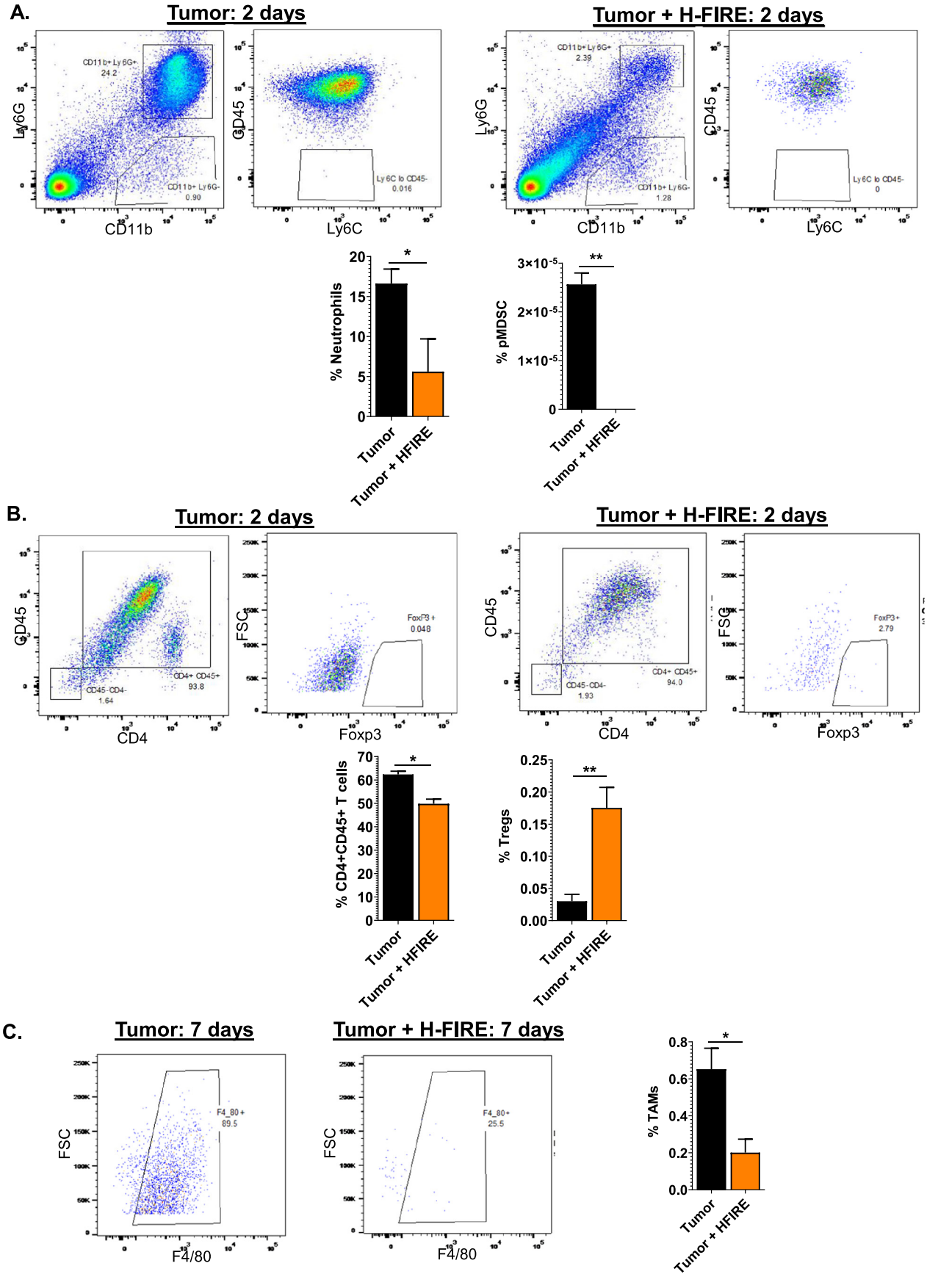
A.
Tumor: 2 days
Tumor + H-FIRE: 2 days
CD11b+ Ly 6G+
24.2
CD11b+ Ly 6G-
0.90
Ly6G
CD11b
CD45
Ly6C
Ly 6C lo CD45-
0.016
CD11b+ Ly 6G+
2.39
CD11b+ Ly 6G-
1.28
Ly 6C lo CD45-
0
% Neutrophils
% pMDSC
Tumor
Tumor + HFIRE
B.
Tumor: 2 days
Tumor + H-FIRE: 2 days
CD45-CD4-
1.64
CD4+ CD45+
93.8
CD4
FSC
Foxp3
FoxP3+
0.048
CD45-CD4-
1.93
CD4+ CD45+
94.0
FoxP3+
2.79
% CD4+CD45+ T cells
% Tregs
C.
Tumor: 7 days
Tumor + H-FIRE: 7 days
F4_80+
89.5
F4_80+
25.5
F4/80
% TAMs

hypothesized that H-FIRE treatment improves these functions. The predominantly non-thermal mechanism of H-FIRE likely generates novel neoantigens from the 4 T1 cells in their native form that are not heat or cold denatured. This is expected to improve antigen recognition and would be consistent with the metastasis data described above. We also anticipate the prolonged cell death associated with H-FIRE allows antigen generation and presentation to occur over an extended period of time, further enhancing APC exposure and sampling. To evaluate this hypothesis, we treated 4 T1 cells *in vitro* using 2000 V/cm H-FIRE or treated cells using cryoablation involving 3 rounds of cooling in liquid Nitrogen for 30 s followed by rapid recovery at 37 °C for 3 min (modified from [43]). Following 24-h recovery, cell suspensions were filtered to remove any remaining 4 T1 cells, and the resultant cell-free lysate was i.v.-injected into healthy BALB/c mice. After 10 days, mice were injected with 1.2×10^6 4 T1 cells into a single mammary fat pad, tumor progression was monitored, and tumor diameter was reported at day 30 (Fig. 6F). Control mice i.v.-injected with lysate that did not receive the 4 T1 mammary injection ("lysate only"), did not show any clinical signs of local or systemic tumor progression (Fig. 6F). As expected, mice that received sham treated lysate and 4 T1 mammary injection ("tumor only") demonstrated typical tumor progression (Fig. 6F). Mice that received the 4 T1 lysate following cryoablation demonstrated more variability in tumor progression, but primary tumor size at harvest did not significantly differ from the tumor only group (0.91 ± 0.02 cm *vs.* 0.89 ± 0.06 cm, respectively) (Fig. 6F). Whereas, mice that received lysate from H-FIRE-treated cells demonstrated a statistically significant reduction in tumor size (0.74 ± 0.04 cm) compared to both the tumor only and the cryoablation lysate groups (Fig. 6F). Tumors from mice treated with H-FIRE lysate were 19% reduced compared to tumor only animals and 17% reduced compared to cyroablation lysate (Fig. 6F). In addition to the improvement in primary tumor progression, mice treated with either cryoablation lysate or H-FIRE lysate demonstrated a significant decrease in circulating blood metastatic cells compared to the tumor only group (Fig. 6G). Together, these data indicate that H-FIRE treatment is effective in generating neoantigens that can stimulate the immune system, which contributes to attenuated mammary tumor progression.

4. Discussion

In previous studies by our research team utilizing IRE to treat mouse 4 T1 cells or human MDA-MB-231 cancerous mammary cells, the effects of varying pulse parameters were evaluated on a selection of cell signaling mediators and general assessments of cell death [23,44]. The current work expands these data to a more comprehensive assessment of the tumor microenvironment and hallmarks of tumorigenesis following a novel electroporation strategy. Here, we show that H-FIRE initiates inflammatory cell death signaling and a shift in the tumor microenvironment from anti-inflammatory to pro-inflammatory *in vitro* and *in vivo*. Defining the mechanism of cell death as necrosis and pyroptosis is an important distinction, as previous studies have associated IRE with apoptosis [28–31], considered a non-inflammatory form of cell death. Although we observed expression consistent with apoptosis within the first hours post-H-FIRE treatment, cell death shifted to necrosis and pyroptosis over time (Fig. 1). We identified the production of DAMPs ROS, ATP, and HMGB1 as likely contributors to both the shift towards a pro-inflammatory microenvironment and the related shift towards necrosis/pyroptosis (Fig. 1). HMGB1 and ATP, along with calreticulin, were also implicated in electroporation-mediated cell death following NPS in 4T1 cells [24]. Similar to our present study, NPS detected high levels of inflammatory cell death, ultimately resulting in increased activation of dendritic cells [24]. All four mediators (ATP, HMGB1, ROS, and calreticulin) function as DAMPs and activate the NLRP3 inflammasome [45–48], which is a likely mechanism underlying these observations.

As with previous electroporation-based tumor ablation studies in other cancer types, H-FIRE was effective in ablating murine mammary tumors. However, we observed a range of responses we classified as low, average, and high responses. In clinical applications of IRE, computational modeling is used to map and plan treatment for each individual patient, leading to improved ablation zone coverage [49–52]. We did not model electrode placement in the mouse studies due to experimental limitations. Thus, this likely resulted in partial tumor coverage in the treatment zones of some animals. However, our data reveal a significant correlation between activation of the innate immune system and cellular immunity with ablation response, including the identification of a selection of genes and biological functions that are associated with effective H-FIRE tumor ablation (Fig. 4). It is interesting to speculate that identification of specific cellular immunity genes correlated with favorable treatment responses could be further developed and leveraged as biomarker/s of H-FIRE responsiveness, or lack of therapeutic responsiveness, in human patients.

Early studies evaluating IRE and related electroporation techniques used human cancer cell lines implanted into immunocompromised mice [53–55]. These studies were critical to explore tumor ablation in human-relevant cancers, but the lack of a functional immune system missed key elements of the host response to treatment. In one of the few studies directly comparing immunocompetent (BALB/c) *versus* immunodeficient (nude) mice, IRE treatment of subcutaneous renal tumors was more effective in BALB/c mice, requiring 60% less voltage for complete regression compared to nude animals [56]. These findings are similar to ours, where H-FIRE treatment was more effective in ablating the primary tumor in BALB/c mice compared to NSG animals (Figs. 2 and 6). Interestingly, Neal et al., re-injected animals with the same renal cell line 18 days post-IRE treatment and found attenuation of secondary tumor growth in immunocompetent mice [56]. Similar findings were also reported for animals following NPS in the 4T1 model [24]. Together, these data suggest engagement of the adaptive immune system that is consistent with our findings following the pre-treatment of animals with the lysate from H-FIRE treated 4T1 cells (Fig. 6). Based on these data, we believe that ablation modalities such as H-FIRE, which produces minimal heating under relevant treatment scenarios, have negligible effects on protein structure and folding, improving antigen presentation and recognition. We believe these data illustrate the potential for H-FIRE to engage the adaptive immune system and promote immunological memory that could be harnessed to minimize tumor progression and prevent recurrence.

One of the most striking findings from these studies reveals that local treatment with H-FIRE can significantly impact metastasis (Fig. 6). We observed reduced lung and blood metastases in H-FIRE-treated animals. These findings are complementary to recent NPS studies, which induced similar levels of anti-tumor immunity and reduced distant organ metastases in the 4T1 model [24]. Following NPS, the authors focused on assessments of systemic leukocytes, and found that NPS induced long-term memory T cells and reduced circulating Tregs [24]. We evaluated the cell populations as described in this study, but did not observe these changes post-H-FIRE (data not shown). However, this is not surprising as our study focused on earlier timepoints and changes in the local tumor microenvironment. We detected the biggest differences in local cell populations, rather than circulating/systemic populations, and observed reduced TANs, MDSCs, and TAMs in the

Fig. 5. H-FIRE Treatment Significantly Alters Local Immune Cell Populations in the 4 T1 Tumor Microenvironment. Mice were treated with H-FIRE and tumors were harvested at 2 and 7 days post-treatment. Single cell suspensions were generated from each tumor and labeled for flow cytometry. A. 2 days after H-FIRE, the treated groups showed significant reduction in $CD11b^+LY6G^+$ cells, representing neutrophil populations, and $CD11b^+LY6G^+Ly6C^{lo}CD45^-$ cells, representing pMDSC populations. B. Significant decreases were observed in $CD4^+CD45^+$ T helper cells, while significant increases were observed in $CD4^+CD45^+CD25^{hi}CD127^{lo}Foxp3^+$ Treg population. C. $CD11b^+Ly6G^-Ly6C^-CD45^+F4/80^+$ Tumor Associated Macrophage populations were significantly decreased 7 days post-treatment. $n = 4$ mice in each group. $^*p \le 0.05$; $^{**}p \le 0.01$.

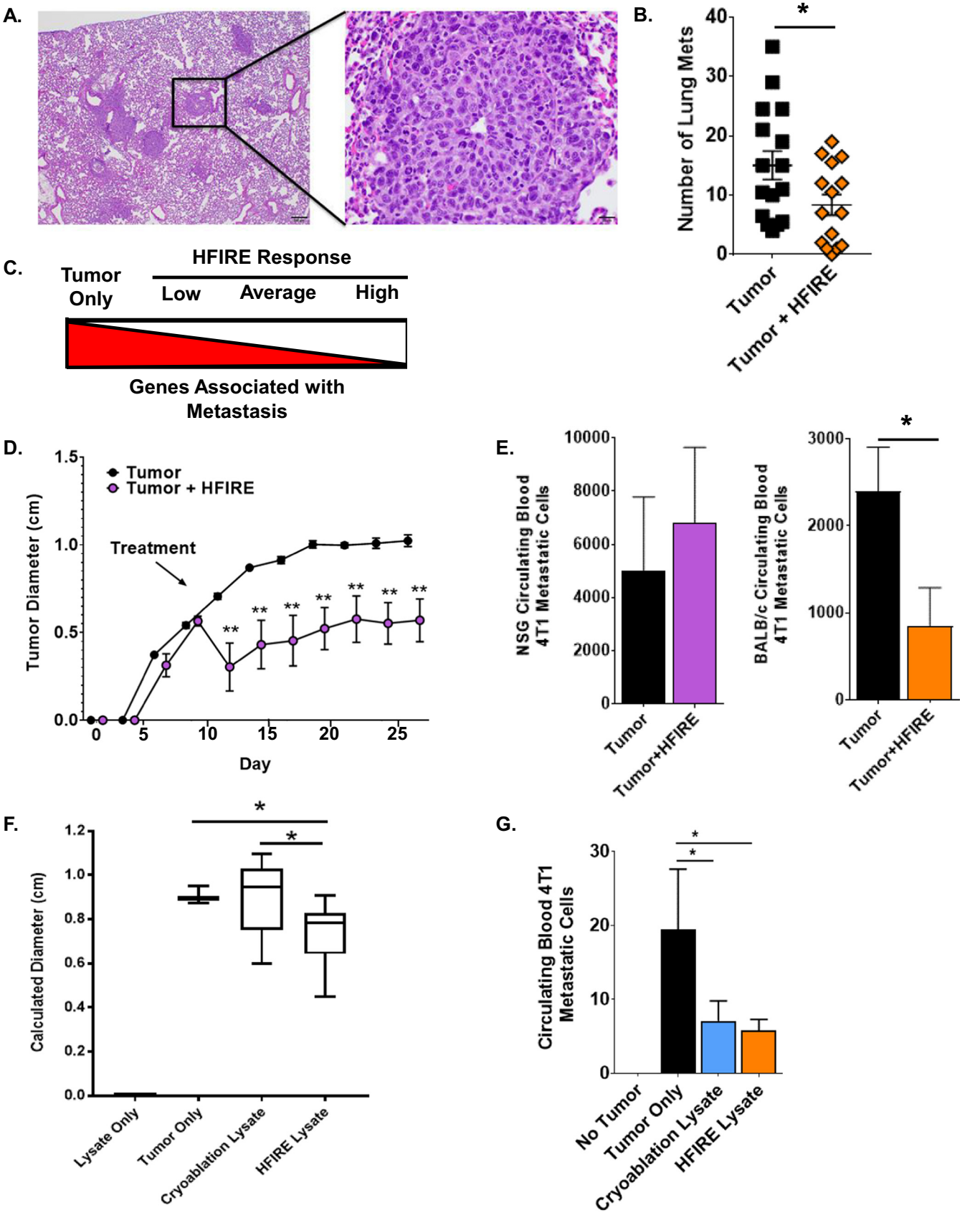

tumor microenvironment following treatment. NPS and H-FIRE are fundamentally different electroporation techniques, but despite mechanistic differences, similar overall clinical and phenotypic results of tumor ablation and systemic anti-tumor immune system activation were observed, emphasizing the utility of electroporation-based therapeutics.

Overall, our data support a model whereby the inflammatory cell death mechanism following H-FIRE increases cellular immune

responses and leukocyte recruitment, improving antigen processing and promoting systemic anti-tumor immunity. The removal of anti-inflammatory components of the tumor microenvironment, including TAN, MDSC, and TAM populations, should make the microenvironment more favorable for combination therapies. Additionally, improved antigen presentation and greater lymphocyte accessibility to the tumor should improve responses to immunotherapeutics, such as checkpoint inhibitors. This is expected to improve ablation of the primary breast tumor, eliminate metastases, and prevent recurrence. It is also likely that the combined therapeutic approach of H-FIRE and immunotherapy may prevent potential tumor expansion that has been observed in previous studies following IRE and other tumor ablation strategies. Using H-FIRE as a pre-treatment to improve immune system activation and surveillance, even in tumors that will ultimately be surgically removed in a treat and resect strategy, may also improve long-term prognosis.

Supplementary data to this article can be found online at https://doi.org/10.1016/j.ebiom.2019.05.036.

Funding sources

This work was supported by the Virginia-Maryland College of Veterinary Medicine (I.C.A.), the Virginia Tech Institute for Critical Technology and Applied Science Center for Engineered Health (I.C.A.), the Virginia Biosciences Health Research Corporation (VBHRC) Catalyst (R.V.D.), and the National Institutes of Health R01CA213423 (R.V.D. and S.S.V.), P01CA207206 (R.V.D and R.V.D.), R56AI127800 (K.J.O.), and R01AI134972 (K.J.O.). Student work on this publication was supported by the National Institute of Allergy and Infectious Diseases Animal Model Research for Veterinarians (AMRV) training grant (T32-OD010430) (S.C.O. and K.E.) and the American Association of Immunologist Careers in Immunology Fellowship Program (V.M.R.S.). The content is solely the responsibility of the authors and does not necessarily represent the official views of the NIH or any other funding agency.

Declaration of interests

I.C.A., M.F.L., N.B.W., S.S.V., J.H.R., and R.V.D. are inventors on pending and issued patents related to the work. Authors declare no other conflicts of interest.

Author contributions

V.M.R.-S. designed, performed the *in vitro* and *in vivo* experiments, analyzed and interpreted the data, prepared the figures, and wrote the paper. N.B.W., M.F.L., and R.V.D. were responsible for designing the H-FIRE treatment parameters. N.B.W. performed the *in vitro* H-FIRE experiments. M.F.L. performed the *in vivo* H-FIRE experiments. R.M.B. performed the *in vitro* cell viability studies. R.M.B., K.E.H., D.K.M., and K.E. assisted with live animal monitoring and necropsy. S.C.-O. and K.E. read all the H&E slides and provided scoring and expertise on the methods and results. S.S.V., J.H.R., K.J.O., R.V.D., and I.C.A. provided expertise on the design of the studies, interpretation of results, and revisions to the manuscript. I.C.A. provided overall direction, generated the IPA figures, and wrote the manuscript. All authors have read and approved the manuscript.

Acknowledgements

We would like to acknowledge Dr. Robert C.G. Martin II for providing clinical insight related to this manuscript. We would also like to acknowledge undergraduate students that assisted with aspects of this manuscript, including Cassidy Thomas, Maia Tatum, and Jenna Coulturi. Dr. Daniel Rothschild assisted with live animal images. Dr. Catharine Cowan and Melissa Makris of our Flow Cytometry Core provided technical assistance with this aspect of the study. We would also like to acknowledge the staff and personnel related to our Teaching and Research Animal Care Support Service (TRACSS). Center support was provided by the Virginia Tech Center for Engineered Health and the Virginia Tech Institute for Critical Technology and Applied Science.

References

[1] DeSantis C, et al. Breast cancer statistics, 2013. CA Cancer J Clin 2014;64(1):52–62.
[2] Xiao W, et al. Breast cancer subtypes and the risk of distant metastasis at initial diagnosis: a population-based study. Cancer Manag Res 2018;10:5329–38.
[3] Vikas P, Borcherding N, Zhang W. The clinical promise of immunotherapy in triple-negative breast cancer. Cancer Manag Res 2018;10:6823–33.
[4] Garcia-Tejedor A, et al. Radiofrequency ablation followed by surgical excision versus lumpectomy for early stage breast Cancer: a randomized phase II clinical trial. Radiology 2018;289(2):317–24.
[5] Thomson KR, Kavnoudias H, Neal RE. Introduction to irreversible electroporation–principles and techniques. Tech Vasc Interv Radiol 2015;18(3):128–34.
[6] Coelen RJS, et al. Ablation with irreversible electroporation in patients with advanced perihilar cholangiocarcinoma (ALPACA): a multicentre phase I/II feasibility study protocol. BMJ Open 2017;7(9):e015810.
[7] Garcia PA, et al. Non-thermal irreversible electroporation (N-TIRE) and adjuvant fractionated radiotherapeutic multimodal therapy for intracranial malignant glioma in a canine patient. Technol Cancer Res Treat 2011;10(1):73–83.
[8] Hong Y, et al. The use of IRE in multi-modality treatment for oligometastatic pancreatic cancer. Am J Surg 2018;216(1):106–10.
[9] Rodriguez A, Tatter SB, Debinski W. Neurosurgical techniques for disruption of the blood-brain barrier for glioblastoma treatment. Pharmaceutics 2015;7(3):175–87.
[10] Rossmeisl JH, et al. Safety and feasibility of the NanoKnife system for irreversible electroporation ablative treatment of canine spontaneous intracranial gliomas. J Neurosurg 2015;123(4):1008–25.
[11] Ruarus AH, et al. Irreversible electroporation in Hepatopancreaticobiliary Tumours. Can Assoc Radiol J 2018;69(1):38–50.
[12] Savic LJ, et al. Irreversible electroporation in interventional oncology: where we stand and where we go. Rofo 2016;188(8):735–45.
[13] Scheffer HJ, et al. Irreversible electroporation for nonthermal tumor ablation in the clinical setting: a systematic review of safety and efficacy. J Vasc Interv Radiol 2014;25(7):997–1011 [quiz 1011].
[14] Scheffer HJ, et al. Ablation of locally advanced pancreatic cancer with percutaneous irreversible electroporation: results of the phase I/II PANFIRE study. Radiology 2017;282(2):585–97.
[15] Scheffer HJ, et al. Colorectal liver metastatic disease: efficacy of irreversible electroporation–a single-arm phase II clinical trial (COLDFIRE-2 trial). BMC Cancer 2015;15:772.
[16] Tarantino L, et al. Irreversible electroporation of locally advanced solid pseudopapillary carcinoma of the pancreas: a case report. Ann Med Surg (Lond) 2018;28:11–5.
[17] Arena CB, et al. High-frequency irreversible electroporation (H-FIRE) for non-thermal ablation without muscle contraction. Biomed Eng Online 2011;10:102.
[18] Sanchez K, Page D, McArthur HL. Immunotherapy in breast cancer: an overview of modern checkpoint blockade strategies and vaccines. Curr Probl Cancer 2016;40(2–4):151–62.
[19] Lee EW, Thai S, Kee ST. Irreversible electroporation: a novel image-guided cancer therapy. Gut Liver 2010;4(Suppl. 1):S99–S104.

Fig. 6. Local H-FIRE Treatment Attenuates Metastatic Lesions in Immunocompetent mice. Lung and blood metastasis is typical in the 4 T1 tumor model. A. Histopathology evaluation of the lungs revealed 4 T1 metastatic lesions in all of the animals that were not treated with H-FIRE. B. Pathologic enumeration of metastatic lesions revealed a significant decrease in lung metastases in animals 15 days post-H-FIRE treatment compared to untreated animals. C. Gene expression in the primary tumor post-H-FIRE revealed a significant decrease in signaling pathways associated with tumor metastasis in animals with tumors that were highly responsive to H-FIRE ablation. D-E. Metastasis attenuation depends on an intact immune system. NOD Scid Gamma (NSG) mice were injected with 1.2×10^6 4T1 cells into the mammary fat pad, treated with H-FIRE (2–5-2 waveform, 2500 V/cm), and tumor progression was monitored. D. A significant attenuation in tumor progression was observed in the NSG mice; however, no tumors reached complete ablation. E. Whole blood was collected from both NSG and BALB/c mice and plated under 6-thioguanine selection. A significant number of metastatic cells were observed in the NSG mice, regardless of H-FIRE treatment. In the BALB/c mice, a significant reduction in average circulating 4 T1 metastatic cells was observed in animals treated with H-FIRE. F-G. 4 T1 cells were treated with either H-FIRE (2–5-2 waveform, 2000 V/cm) or cryoablation (liquid Nitrogen to 37 °C, 3 freeze-thaw cycles). Cell-free lysates were generated and injected (i.v.) into wild type BALB/c mice. Mice were injected with 1.2×10^6 4T1 cells into the mammary fat pad 10 days post-injection of cell-free lysate. F. At necropsy, the calculated tumor diameter of mice treated with the H-FIRE lysate was significantly decreased compared to both untreated tumor only (19% reduction) and cryoablation lysate (17% reduction). G. Circulating blood 4 T1 metastatic cells were quantified at necropsy. Both cyroablation lysate and H-FIRE lysate treatment significantly attenuated 4T1 metastasis. n = 3–10 mice in each group. *$p \le 0.05$; **$p \le 0.01$.

[20] Lencioni R, Crocetti L. Image-guided ablation for hepatocellular carcinoma. Recent Results Cancer Res 2013;190:181–94.
[21] Lv Y, Zhang Y, Rubinsky B. Molecular and histological study on the effects of electrolytic electroporation on the liver. Bioelectrochemistry 2019;125:79–89.
[22] Zhao J, et al. Irreversible electroporation reverses resistance to immune checkpoint blockade in pancreatic cancer. Nat Commun 2019;10(1):899.
[23] Goswami I, et al. Irreversible electroporation inhibits pro-cancer inflammatory signaling in triple negative breast cancer cells. Bioelectrochemistry 2017;113:42–50.
[24] Guo S, et al. Nano-pulse stimulation induces potent immune responses, eradicating local breast cancer while reducing distant metastases. Int J Cancer 2018;142(3):629–40.
[25] Pulaski BA, Ostrand-Rosenberg S. Mouse 4T1 breast tumor model. Curr Protoc Immunol 2001;20:2.
[26] Vogel JA, et al. Time-dependent impact of irreversible electroporation on pancreas, liver, blood vessels and nerves: a systematic review of experimental studies. PLoS One 2016;11(11):e0166987.
[27] Lundt JE, et al. Non-invasive, rapid ablation of tissue volume using histotripsy. Ultrasound Med Biol 2017;43(12):2834–47.
[28] Zhang H, et al. High-voltage pulsed electric field plus photodynamic therapy kills breast cancer cells by triggering apoptosis. Am J Transl Res 2018;10(2):334–51.
[29] Kim HB, et al. Changes of apoptosis in tumor tissues with time after irreversible electroporation. Biochem Biophys Res Commun 2013;435(4):651–6.
[30] Long G, et al. Histological and finite element analysis of cell death due to irreversible electroporation. Technol Cancer Res Treat 2014;13(6):561–9.
[31] Zhang Z, et al. Rapid dramatic alterations to the tumor microstructure in pancreatic cancer following irreversible electroporation ablation. Nanomedicine (Lond) 2014;9(8):1181–92.
[32] Man SM, Karki R, Kanneganti TD. Molecular mechanisms and functions of pyroptosis, inflammatory caspases and inflammasomes in infectious diseases. Immunol Rev 2017;277(1):61–75.
[33] Deng M, et al. The endotoxin delivery protein HMGB1 mediates Caspase-11-dependent lethality in sepsis. Immunity 2018;49(4):740–53.
[34] Zhou B, et al. Tom20 senses iron-activated ROS signaling to promote melanoma cell pyroptosis. Cell Res 2018;28(12):1171–85.
[35] Zha QB, et al. ATP-induced Inflammasome activation and Pyroptosis is regulated by AMP-activated protein kinase in macrophages. Front Immunol 2016;7:597.
[36] Sano MB, et al. Bursts of bipolar microsecond pulses inhibit tumor growth. Sci Rep 2015;5:14999.
[37] Sweeney DC, et al. Quantification of cell membrane permeability induced by monopolar and high-frequency bipolar bursts of electrical pulses. Biochim Biophys Acta 2016;1858(11):2689–98.
[38] Mercadal B, et al. Avoiding nerve stimulation in irreversible electroporation: a numerical modeling study. Phys Med Biol 2017;62(20):8060–79.
[39] Benevides L, et al. IL17 promotes mammary tumor progression by changing the behavior of tumor cells and eliciting tumorigenic neutrophils recruitment. Cancer Res 2015;75(18):3788–99.
[40] Murugaiyan G, Saha B. Protumor vs antitumor functions of IL-17. J Immunol 2009;183(7):4169–75.
[41] Kim K, et al. Eradication of metastatic mouse cancers resistant to immune checkpoint blockade by suppression of myeloid-derived cells. Proc Natl Acad Sci U S A 2014;111(32):11774–9.
[42] de Gruijl T, Stam AG. From local to systemic treatment: leveraging antitumor immunity following irreversible electroporation. Irreversible Electroporation Clin Practice 2018:249–70.
[43] Alaniz L, Rizzo MM, Mazzolini G. Pulsing dendritic cells with whole tumor cell lysates. Methods Mol Biol 2014;1139:27–31.
[44] Neal RE, Davalos RV. The feasibility of irreversible electroporation for the treatment of breast cancer and other heterogeneous systems. Ann Biomed Eng 2009;37(12):2615–25.
[45] Allen IC, et al. The NLRP3 inflammasome mediates in vivo innate immunity to influenza A virus through recognition of viral RNA. Immunity 2009;30(4):556–65.
[46] Mariathasan S, et al. Cryopyrin activates the inflammasome in response to toxins and ATP. Nature 2006;440(7081):228–32.
[47] Willingham SB, et al. NLRP3 (NALP3, Cryopyrin) facilitates in vivo caspase-1 activation, necrosis, and HMGB1 release via inflammasome-dependent and -independent pathways. J Immunol 2009;183(3):2008–15.
[48] Fang L, et al. Involvement of endoplasmic reticulum stress in albuminuria induced inflammasome activation in renal proximal tubular cells. PLoS One 2013;8(8):e72344.
[49] van den Bos W, et al. The correlation between the electrode configuration and histopathology of irreversible electroporation ablations in prostate cancer patients. World J Urol 2016;34(5):657–64.
[50] Scheltema MJ, et al. Irreversible electroporation for the treatment of localized prostate cancer: a summary of imaging findings and treatment feedback. Diagn Interv Radiol 2017;23(5):365–70.
[51] Zupanic A, Kos B, Miklavcic D. Treatment planning of electroporation-based medical interventions: electrochemotherapy, gene electrotransfer and irreversible electroporation. Phys Med Biol 2012;57(17):5425–40.
[52] Fuhrmann I, et al. Navigation systems for treatment planning and execution of percutaneous irreversible electroporation. Technol Cancer Res Treat 2018;17:1533033818791792.
[53] Neal 2nd RE, et al. Treatment of breast cancer through the application of irreversible electroporation using a novel minimally invasive single needle electrode. Breast Cancer Res Treat 2010;123(1):295–301.
[54] Jose A, et al. Irreversible electroporation shows efficacy against pancreatic carcinoma without systemic toxicity in mouse models. Cancer Lett 2012;317(1):16–23.
[55] Su JJ, et al. Histological analysis of human pancreatic carcinoma following irreversible electroporation in a nude mouse model. World J Gastrointest Oncol 2018;10(12):476–86.
[56] Neal 2nd RE, et al. Improved local and systemic anti-tumor efficacy for irreversible electroporation in immunocompetent versus immunodeficient mice. PLoS One 2013;8(5):e64559.